Numerical study of spatio-temporal dynamics in all semiconductor PCSELs

Lilli Kuen*, Eduard Kuhn*, Hans Wenzel†, Paul Crump†, and Mindaugas Radziunas*
*Weierstrass Institute (WIAS), Mohrenstrasse 39, 10117 Berlin, Germany. Email: lillifriederike.kuen@wias-berlin.de
†Ferdinand-Braun-Institut (FBH), Gustav-Kirchhoff-Str. 4, 12489 Berlin, Germany.

***Abstract*—We present a numerical study of all semiconductor photonic crystal surface-emitting lasers with two types of photonic crystals. We utilize time-domain simulations that are performed using the three-dimensional coupled-wave theory. Our evaluation includes examining carrier density, output power, optical spectra, near- and far-field.**

Photonic crystal (PC) surface-emitting lasers (SELs), see Fig. 1(a), are devices engineered to achieve single-mode operation and a narrow far-field emission pattern by utilizing a photonic crystal structure [1]. Typically, these lasers explore a two-dimensional (2D) PC layer with a-periodic air voids in both lateral directions (x and y), where the lattice constant a defines the edge length of the square unit cell of the PC. The best to date high-power PCSELs [2] rely on the PCs defined by a pair of elliptic features located along the diagonal of the unit cell. It is expected that such devices should enable continuous wave operation in a single-mode [3]. In this work, we present the design of an *all-semiconductor*

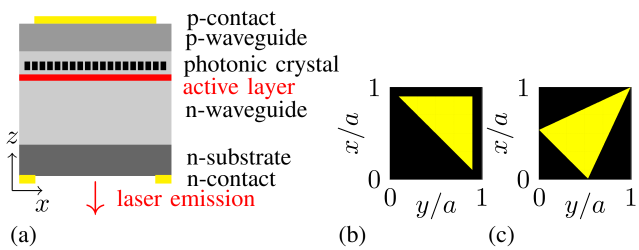

Fig. 1. Cross-section of a PCSEL based on [8] (a), rectangular isosceles triangle (RIT) feature (b), and stretched isosceles triangle (SIT) feature (c).

PCSEL featuring a PC layer composed of isosceles triangular InGaP features embedded within a GaAs matrix, see Figs. 1(b) and 1(c). Through dynamic simulations, we demonstrate that a proper choice of triangles, following the proposal of [4], can enable stable single-mode lasing in PCSELs with emission areas exceeding several mm^2 [5].

We use the three-dimensional coupled-wave theory [6], [7] to simulate the dynamical behavior of PCSELs within the in-domain plain $Q_L = [0, L] \times [0, L]$. The complex field $\mathbf{E}$ consists of four components, the slowly varying complex field amplitudes propagating in $\pm x$- and $\pm y$-directions, stated as $\mathbf{E} = \left[E_x^+, E_x^-, E_y^+, E_y^-\right]^T$, respectively. According to [5], [7], the field equations are given as a system of four linear PDEs with according boundary conditions

$$\tfrac{1}{v_{gr}}\partial_t \mathbf{E}(x,y,z) = \left[\mathbf{D} + i\left(\mathbf{C} - \Delta\beta(N)\right)\right]\mathbf{E} + \mathbf{F_{sp}}, \tag{1}$$

$$E_x^+(0,y,t) = E_x^-(L,y,t) = E_y^+(x,0,t) = E_y^-(x,L,t) = 0,$$

$$\mathbf{D} = \begin{pmatrix} \sigma\partial_x & 0 \\ 0 & \sigma\partial_y \end{pmatrix}, \quad \sigma = \begin{pmatrix} -1 & 0 \\ 0 & 1 \end{pmatrix}.$$

Here, v_{gr} and $\mathbf{F_{sp}}$ are the group velocity and the spontaneous emission [8]. $\mathbf{C}$ is the complex $[4 \times 4]$ field coupling matrix [6], [7], depending on the design of the PC and the vertical structure of the PCSEL. The spatially-distributed relative propagation factor $\Delta\beta$ [5], [8] is given by

$$\Delta\beta(N) = k_0\Delta_n(N) + \tfrac{i}{2}\left[g(N) - \alpha - \mathcal{D}\right] \tag{2}$$

with the central wave vector $k_0 = 2\pi/\lambda_0$, central wavelength $\lambda_0 = an_{\text{eff}}$, and the effective refractive index n_{eff}. $\Delta_n(N)$ denotes the refractive index change, $g(N)$ the carrier-dependent logarithmic gain, α the total field loss, and $\mathcal{D}$ is a linear operator modeling the Lorentzian-shaped gain dispersion. This model does not account for dependencies on temperature. Finally, the carrier density $N(x,y,t)$ in the active region is described by the diffusive carrier rate equation [7],

$$\partial_t N = \nabla_\perp \cdot \left(D_N \nabla_\perp\right) N + \tfrac{j}{ed} - R_{sp}(N) - R_{st}(N, \mathbf{E}),$$
$$R_{sp} = \tfrac{N}{\tau_N} + BN^2 + CN^3, R_{st} \propto \Re\left[\mathbf{E}^* \cdot \left(g(N) - \mathcal{D}\right)\mathbf{E}\right], \tag{3}$$

with $\nabla_\perp = [\partial_x, \partial_y]^T$, carrier diffusion D_N, injected current distribution $j(x,y)$, the elementary charge e, thickness of the active zone d, spontaneous emission R_{sp} and stimulated emission R_{st}. To perform time-dependent simulations, (1) and (3) are discretized using finite differences. For more details, see [5], [9].

In our simulations, we use a PCSEL with vertical structure and parameters from [5], [8], a sketch is given in Fig. 1(a). The PCSEL is of size $L = 2.4\,\text{mm}$ with a circular contact with diameter $D = 1.6\,\text{mm}$. We explore the following features of the PC: a rectangular isosceles triangle (RIT), as shown in Fig. 1(b) and considered in [8] and [6], and a stretched isosceles triangle (SIT), as shown in Fig. 1(c) and first introduced in [4]. During time integration, we use discretization steps $h = 9.6\,\mu\text{m}$ in space and $\Delta t = h/v_{gr} \approx 0.12\,\text{ps}$ in time.

The carrier density and the output power of the time-dependent simulations are shown for both PCSELs in Fig. 2.

This work was performed in the frame of the German Leibniz Association funded project "PCSELence" (K487/2022).

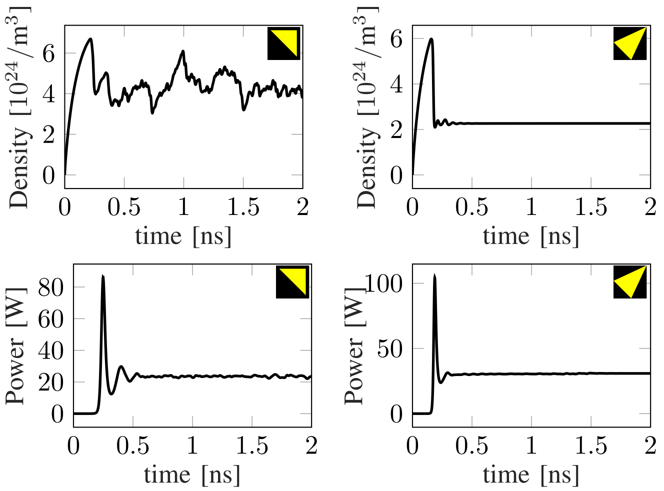

Fig. 2. Carrier density and optical output power for the RIT-PCSEL on the left and the SIT-PCSEL on the right side. The oscillation is part of the switching-on behavior of the laser; after about 1.5 ns, the stabilization of the transients is reached. Top-right corner insets represent the corresponding PC features.

In the case of RIT, see the left part of Fig. 2, the carrier density shows never-vanishing fluctuations, determined by the interaction of multiple modes. In comparison, for the SIT in the right part of Fig. 2, the carrier density and the output power reached by a single fundamental mode converge to a steady state in approximately 1.5 ns. The optical spectra and far-field for both structures are presented in Fig. 3. For the RIT-PC-based PCSEL case, the far-field shows several side lobes in addition to the main peak in the center, while the far-field of the SIT-PCSEL consists of a single spot in the center. This is also visible in the optical spectra. In the case of the RIT-PCSEL, the shift is $\Delta\lambda \approx 1.5\,\mathrm{nm}$, and a peak broadened by multiple contributing modes can be observed. This aligns with the multimodal behavior already described for the carrier density. For the SIT-PCSEL, one main peak exists, slightly above $\Delta\lambda = 0$. The time-averaged near-field distributions for both PCSELs are depicted in Fig. 4. The RIT-PCSEL shows the emission pattern corresponding to the contact shape, exhibiting multiple small-scale intensity fluctuations. In contrast, the SIT-PCSEL shows a much smoother profile with decreasing intensity to the sides. The degradation from a perfectly circular beam profile is the result of a phase mismatch between counterpropagating fundamental mode components.

In conclusion, we have performed time-domain simulations using a 3D-TW model for all semiconductor PCSELs featuring two types of PC. We demonstrated the difference in the time-dependent behavior of both structures. It was shown that the choice of PC features has a crucial impact on the type of operation. Our preliminary simulations show that employing SIT-type PC features can facilitate single-mode lasing in PCSELs with contact areas extending to $10\,\mathrm{mm}^2$ and beyond.

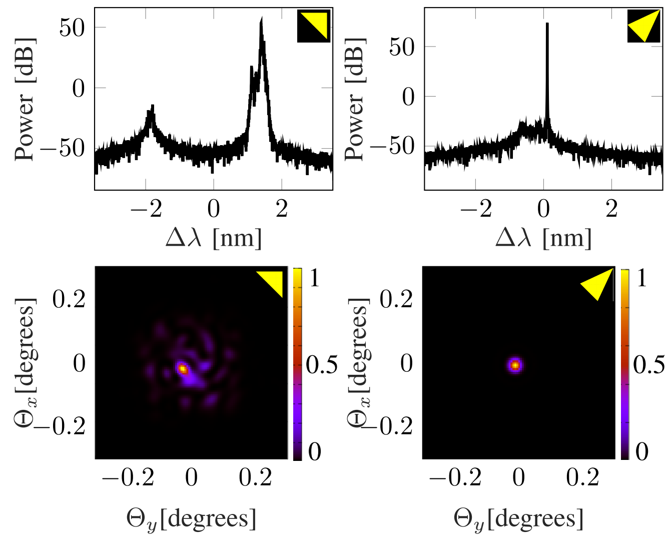

Fig. 3. Optical spectra and far-field on the top side of the PCSEL for the RIT-PCSEL on the left and the SIT-PCSEL on the right side.

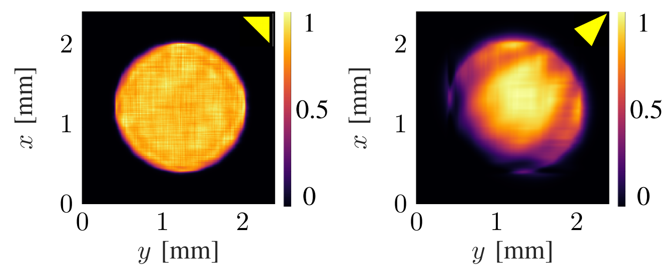

Fig. 4. Time-averaged near-field on the bottom side of the PCSEL for a RIT-PCSEL on the left and a SIT-PCSEL on the right side.

References

[1] S. Noda, K. Kitamura, T. Okino et al., "Photonic-crystal surface-emitting lasers: Review and introduction of modulated-photonic crystals," IEEE J. Sel. Top. Quantum Electron. **23**, 4900107, 2017.

[2] M. Yoshida, S. Katsuno, T. Inoue et al., "High-brightness scalable continuous-wave single-mode photonic-crystal laser," Nature **618**, 727, 2023.

[3] T. Inoue, M. Yoshida, J. Gelleta et al., "General recipe to realize photonic-crystal surface-emitting lasers with 100-W-to-1-kW single-mode operation," Nat. Commun. **13**, 3262, 2022.

[4] B. King, H. Wenzel, E. Kuhn et al., "Design of very-large area photonic crystal surface emitting lasers with an all-semiconductor photonic crystal," Opt. Express **32**, 44945, 2024.

[5] M. Radziunas, H. Wenzel, B. King et al., "Dynamical simulations of single-mode lasing in large-area all-semiconductor PCSELs", Opt. Lett. **50**, 1953, 2025.

[6] Y. Liang, C. Peng, K. Sakai et. al., "Three–dimensional coupled–wave analysis for square–lattice photonic crystal surface emitting lasers with transverse–electric polarization: finite–size effects," Opt. Express **20**, 15945, 2012.

[7] T.Inoue, R. Morita, M. Yoshida et al., "Comprehensive analysis of photonic-crystal surface-emitting lasers via time-dependent three-dimensional coupled-wave theory," Phys. Rev. B **99**, 035308, 2019.

[8] H. Wenzel, E. Kuhn, B. King et al., "Theory of the linewidth-power product of photonic-crystal surface-emitting lasers," IEEE J. Quantum Electron. **61**, 2400114, 2025.

[9] M. Radziunas, E. Kuhn, and H. Wenzel, "Solving a spectral problem for large-area photonic crystal surface-emitting lasers", Math. Model. Anal. **29**, 575, 2024.